ISSN: 1410-8917
Jurnal Kimia Sains & Aplikasi
e-ISSN: 2597-9914

Jurnal Kimia Sains dan Aplikasi 25 (10) (2022): 362–367

Jurnal Kimia Sains dan Aplikasi
Journal of Scientific and Applied Chemistry

Journal homepage: http://ejournal.undip.ac.id/index.php/ksa

Effect of the Amount of Carbon in the Fe_3O_4@ZnO-C Nanocomposites on Its Structure and Magnetic Properties

Astuti [a,*], Syukri Arief [b], Devi Pebrina [a]

[a] Department of Physics, Faculty of Sciences and Mathematics, Andalas University, Padang, Indonesia
[b] Department of Chemistry, Faculty of Sciences and Mathematics, Andalas University, Padang, Indonesia

* Corresponding author: astuti@sci.unand.ac.id

https://doi.org/10.14710/jksa.25.10.362-367

Article Info

Article history:

Received: 28th September 2022
Revised: 23rd November 2022
Accepted: 23rd December 2022
Online: 25th December 2022

Keywords:
Fe_3O_4@ZnO nanocomposite; coprecipitation; magnetic properties; carbons

Abstract

Synthesis and characterization of structure magnetic properties of Fe_3O_4@ZnO- C nanocomposite have been done through the precipitation method. This study aimed to discover the effect of concentrations/thickness of carbon layer on crystal structure and magnetic properties of Fe_3O_4@ZnO-C nanocomposites. Fe_3O_4 and Fe_3O_4@ZnO were the samples used in the study, and variations in the amount of carbon were 0.2, 0.1, and 0.05 g. Nanocomposites were characterized using X-ray diffraction (XRD), Fourier-transform infrared spectroscopy (FTIR), and vibrating sample magnetometer (VSM). Based on the results of XRD, it has been found that the crystal structure for Fe_3O_4 was cubic, while ZnO was hexagonal wurtzite. The addition of carbons to Fe_3O_4@ZnO caused a broadening of the diffraction peaks and a decrease in the degree of crystallinity. The bonds formed on Fe_3O_4@ZnO-C nanocomposites, i.e. Fe-O bonds indicated the formation of Fe_3O_4, Zn-O bonds showed the formation of ZnO and C-O, C-H, and O-H bonds revealed the presence of a carbon layer originated from glucose. The VSM results showed that the magnetic saturation decreased with increasing carbon mass. Overall, the carbon-coated nanocomposite material with a carbon mass variation of 0.2, 0.1, and 0.05 g showed superparamagnetic properties with a magnetic saturation of 18.23 emu/g, 19.33 emu/g and 22.05 emu/g, while for the coercive field of 92.29 Oe, 92.90 Oe and 89.60 Oe, respectively. Based on these characterization results, Fe_3O_4@ZnO-C nanocomposite materials can potentially be developed as biomedical materials, such as the materials for photothermal therapy for cancer cells.

1. Introduction

Material applications in the biomedical field have been widely conducted, including diagnostic materials, therapies, and many more. Some diagnostic methods, such as fluorescence imaging (FL), photoacoustic imaging (PAI), and magnetic resonance imaging (MR), have been explored to enhance the accuracy and efficiency during treatment. At the same time, materials for therapies include photothermal therapy, chemical therapy, and others. Gadolinium-based contrast agents are the most commonly used. However, a high-dosage application can be toxic and cause side effects, such as skin thickening, soft tissue calcification, and impaired mobility. Iron oxide (Fe_3O_4) nanoparticles are more promising to be developed than gadolinium-based contrast agents because Fe_3O_4 has better biocompatibility and pharmacokinetics [1, 2].

In the last decade, studies about these biomedical materials have focused more on Fe_3O_4-based since they are biocompatible, easy to synthesize, and can be combined with other nanocomposite materials [2,3]. In biomedical applications, Fe_3O_4 can be combined with other materials, such as luminescence materials or biocompatible materials [3, 4]. Types of luminescence materials that are being used include those from the cluster. The kinds of luminescence materials used are from the groups of lanthanide [5, 6], metal-semiconductor [7, 8], and carbon/graphene [9, 10, 11].

ZnO is one of the luminescent components of the metal semi-conductors group. ZnO is approved as a non-toxic material because there is no evidence of carcinogenicity, genotoxicity, or reproductive toxicity in humans [12]. In addition to the luminescence properties associated with the quantum size effect, ZnO nanoparticles combined with magnetic materials can produce magneto-optical materials in the application of bio-imaging materials and other imaging methods. Some biocompatible materials are polymers, including dextran, albumin, polyethylene glycol, and polyvinyl pyrrolidone, which have been used as coating materials on Fe_3O_4 [13]. Folic acid [14], chitosan [15], and silica [16] are examples of other coating materials.

Magnetic nanoparticles coated with organic and inorganic materials might improve stability, dispersion, and functionality. A strong bond (such as a ZnO-based interfacial covalent bond) is more potential to be developed, especially for nanoparticles suspended in a biological liquid, as shown by the core-shell of Fe_3O_4@ZnO nanocomposite [3, 8, 17]. This iron-based nanocomposite is more stable and safe to be in contact with humans than other magnetic nanoparticles. In addition, the surface of ZnO is rich with -OH cluster, which can easily be functionalized with surface engineering by various molecules.

This study conducted a modification on Fe_3O_4@ZnO by coating it with carbon. This study will determine how the carbon layers affect the magnetic properties of the Fe_3O_4@ZnO nanocomposite material, allowing the material to be used in the biomedical area. Fe_3O_4@ZnO was used as a contrast agent, while the outer part (carbon layer) with good hydrophilicity can be used as a photothermal reagent. After being coated with carbon, the entire Fe_3O_4@ZnO-C nanocomposite has good biocompatibility and magnetism that can be developed as bioimaging and phototherapy materials.

2. Experimental

2.1. Materials and Instruments

The materials used in this study were $FeCl_3.6H_2O$ and $FeSO_4.7H_2O$ (Merck), NH_4OH 21% (Bratachem), alcohol 96%, $Zn(NO_3)_2$ (Merck), PEG 1000 (Merck), and glucose. The characterization instrument used was an X-ray diffractometer (XRD, Bruker D8 Advance) to determine the phase and crystal structure. The chemical bonds formed were identified using Fourier Transform Infrared Spectroscopy (FTIR, Nicolet iS50 FTIR), and Vibrating-Sample Magnetometer (VSM, VSM250) was employed to discover the magnetic properties of materials.

2.2. Synthesis of Fe_3O_4@ZnO

The synthesis of Fe_3O_4@ZnO initially started by synthesizing Fe_3O_4 through the coprecipitation method. $FeSO_4.7H_2O$ and $FeCl_3.6H_2O$ with a molar ratio of 1:2 were dissolved in 30 ml of distilled water. The homogeneous solution was added dropwise with 30 ml of NH_4OH, turning the solution black, and subsequently stirred for 120 minutes at 60°C. The solution was precipitated with a permanent magnet and washed three times with distilled water.

Zinc nitrate was dissolved in 100 ml of distilled water, and gradually added 30 ml of NH_4OH. The zinc nitrate solution was mixed into the Fe_3O_4 precipitate and stirred using a magnetic stirrer at 70°C for 24 hours. The solution was precipitated, separated from the solvent, and washed three times using distilled water. The precipitate was then dried using a furnace at 300°C for 2 hours. Finally, the dried precipitate was ground using a mortar and pestle to form Fe_3O_4@ZnO powder.

2.3. Synthesis of Fe_3O_4@ZnO-C

The synthesis of Fe3O4@ZnO-C initially started by synthesizing carbon. A total of 0.53 g of PEG and 1.8 g of glucose (1:2) were dissolved in 25 ml of distilled water. The solution was stirred using a magnetic stirrer for 30 minutes at 450 rpm. The solution was dried in an oven for 3 hours at 300°C to form carbon and ground into powder.

The following synthesis process combined Fe_3O_4@ZnO with carbon. A total of 0.2 g of carbon powder was dissolved into 10 ml distilled water. The carbon solution was then mixed with 0.4 g of Fe_3O_4@ZnO powder, which was then stirred using a magnetic stirrer for an hour at 80-90°C and dried for 3 hours at 250°C. The dried Fe_3O_4@ZnO-C was ground into powder. Further synthesis was conducted similarly for variations in carbon mass of 0.05 g and 0.1 g.

3. Results and Discussion

3.1. The Analysis of Crystal Structure

XRD characterization results were used to determine the structure of Fe_3O_4@ZnO-C nanocomposites. A wavelength (λ) of 0.15418 and 2θ angle of 20–100° were employed in the process. The X-ray diffraction pattern of the tested sample is shown in Figure 1. The diffraction pattern obtained from the sample characterization results was compared with the standard data from the International Center for Diffraction Database (ICDD).

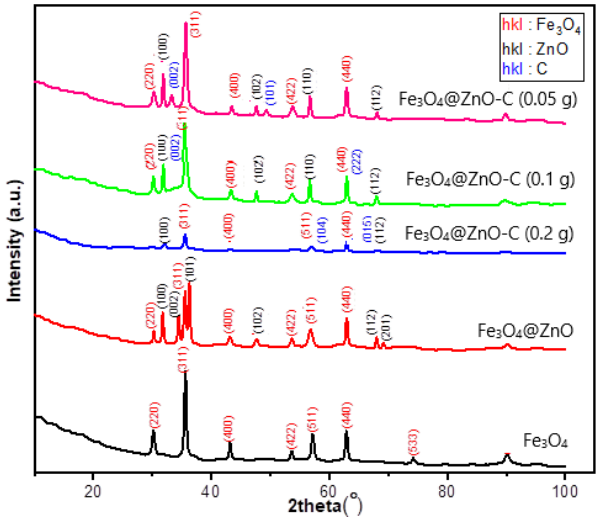

Figure 1. XRD patterns of Fe_3O_4, Fe_3O_4@ZnO and Fe_3O_4@ZnO-C nanocomposites

Based on Figure 1, Fe_3O_4 nanoparticles have a maximum diffraction peak at 2θ = 36.5692°. The results of the Fe_3O_4 synthesis were compared with ICDD standard data with a reference code of 01-088-0315. The indication of the formation of the Fe_3O_4 phase was supported by the appearance of diffraction peaks at Miller indices of (220), (311), (400), (442), (511), (440) and (533). The crystal structure formed was cubic with lattice parameters of a = b = c = 8.3750 Å. Fe_3O_4@ZnO nanocomposite has a maximum diffraction peak at 2θ = 36.2552°. The phase formed from the characterization results is Fe_3O_4 which is characterized by the appearance of a diffraction peak at the Miller indices of (220), (311), (400), (331), (422) and (440), and ZnO phase with Miller indices of (100), (002), (101), (102), (103), (112) and (201), these indicated the successful formation of ZnO shells as supported by the study of Gupta *et al.* [8].

ICDD data with a reference code of 01-088-0315 showed that Fe_3O_4 has a cubic crystal structure with lattice parameters of a = b = c = 8.3750 Å. Meanwhile, ICDD data with a reference code of 01-089-7102 revealed that ZnO has a hexagonal structure with lattice parameters of a = b = 3.2495 Å, and c = 5.2069 Å. Fe_3O_4@ZnO-C nanocomposite with a carbon mass of 0.2 g showed the maximum diffraction peak at an angle of 2θ = 35.527°. The phases formed from the characterization of Fe_3O_4@ZnO-C nanocomposite were Fe_3O_4, ZnO and C. The ICDD data with a reference code of 01-088- 0315 showed that the Fe_3O_4 phase has a cubic crystal structure with lattice parameters of a = b = c = 8.3750 Å. ICDD data with a reference code of 00-001-1136 revealed that the ZnO phase has a hexagonal structure with lattice parameters of a = b = 3.2420 Å and c = 5.1760 Å. The ICDD data with a reference code of 01-073-5918 indicated that phase C has a rhombohedral structure with lattice parameters of a = b = 2.5158 Å and c = 10.2090 Å. Similar to samples with a mass of 0.1 g and 0.05 g carbon, all phases of Fe_3O_4 have a cubic crystal structure, and ZnO has a hexagonal wurtzite crystal structure. Meanwhile, carbon has an orthorhombic structure with lattice parameters of a = 4.5750 Å, b = 5.3040 Å and c = 5.6350 Å, which corresponded to ICDD data with a reference code of 01-089-8488.

Figure 1 also shows that the larger the mass of carbon used, the broader the diffraction peak produced and a decrease in the degree of crystallinity. No peaks corresponding to any other phases are detected, indicating that there has been no reaction between Fe_3O_4, ZnO and C during the coupling of the magnetite core process. As crystalline domain size decreases further, peak broadening increases significantly. The absence of some Fe_3O_4 and ZnO peaks in some samples of Fe_3O_4@ZnO can be attributed to a significant broadening of the peaks, which results in low signal intensity, peak overlapping, and difficulty in peak differentiation. Particles with small crystalline domain sizes become challenging to analyze due to broad peaks and low signal-to-noise ratios, so they are not observable. This can be seen clearly in the Fe_3O_4@ZnO-C nanocomposite sample with a carbon mass of 0.2 g, which in this context might also indicate a decrease in the crystal size of the sample. The crystalline size of Fe_3O_4 nanostructures concerning high-intensity peaks for the crystal plane (311) was estimated using Debye–Scherer's equation (1).

$$D = \frac{0.94\,\lambda}{B\cos\theta} \quad (1)$$

where λ is the wavelength of the X-ray radiation (0.154056 nm), θ is the diffraction angle, and B is the full width of half maximum (FWHM) which can be seen in Table 1.

Table 1 Crystalline size of Fe_3O_4 and Fe_3O_4@ZnO nanocomposites

Sample	B (rad)	cos θ	D (nm)
Fe_3O_4	0.0071	0.952	20.39
Fe_3O_4@ZnO	0.0054	0.950	27.22
Fe_3O_4@ZnO-C (0.2 g)	0.0071	0.952	20.39
Fe_3O_4@ZnO-C (0.1 g)	0.0080	0.952	16.11
Fe_3O_4@ZnO-C (0.05 g)	0.0084	0.952	16.07

Based on Table 1, the size of the Fe_3O_4 crystal was obtained at 20.39 nm, and when merging with ZnO, the crystal was increased to 27.22 nm. The crystal size decreases when nanocomposite Fe_3O_4@ZnO is coated with carbon. The size of the crystal decreases with decreasing amount of carbon utilized. This is because carbon can prevent the movement of nanoparticles to minimize the occurrence of agglomeration [18]. The decrease in crystal size in samples Fe_3O_4@ZnO-C compared to Fe_3O_4 and Fe_3O_4@ZnO causes a decrease in the crystallinity of the nanocomposite, which causes a decrease in magnetic saturation, which is related to the VSM result in Figure 3 [8].

3.2. Functional Group Analysis

FTIR analysis was employed to identify the functional groups present in Fe_3O_4@ZnO nanocomposites by recording spectra in the wavenumber range from 400 to 4500 cm^{-1}. The results of the analysis of the Fe_3O_4@ZnO and Fe_3O_4@ZnO-C nanocomposite functional groups can be seen in Figure 2.

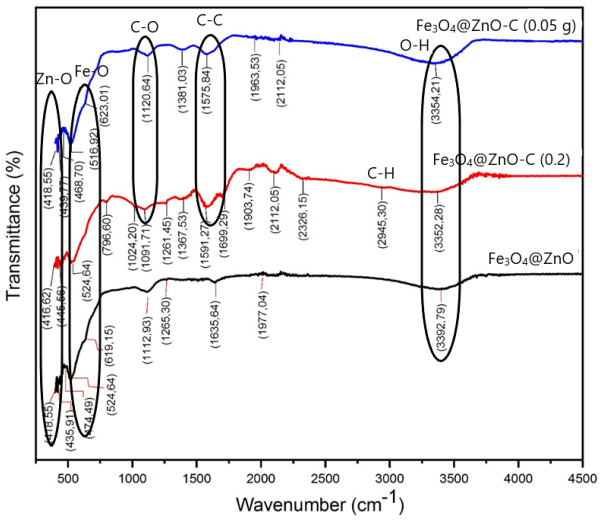

Figure 2. The FTIR spectra of Fe_3O_4@ZnO and Fe_3O_4@ZnO-C nanocomposites

Based on Figure 2, the Fe_3O_4@ZnO nanocomposite shows an absorption peak at 3392.79 cm^{-1}, which is associated with the O-H group indicating the presence of hydrogen bonds and absorption of water molecules on the surface of Fe_3O_4 nanoparticles [19]. The absorption peaks in the 400-500 cm^{-1} range indicate the presence of Zn-O bonds. The absorption bands at 524.64 cm^{-1} and 619.15 cm^{-1} represent the presence of octahedral Fe-O and Fe-O tetrahedral bonds, confirming the formation of Fe_3O_4. The Fe_3O_4@ZnO-C nanocomposite (0.2 g) has a functional group with a C-H bond found at 2945.30 cm^{-1} [18]. The characteristic absorption of the C-C bond at 1591.27 cm^{-1} and 1575.84 cm^{-1} for Fe_3O_4@ZnO-C (0.2 g) and Fe_3O_4@ZnO-C (0.05 g), respectively, showed the presence of a carbon surface, which originated from the inclusive aromatic group in the carbon skeleton [1]. The peak at 1091.71 cm^{-1} and 1120.64 cm^{-1} was associated with the C-O vibration; this possibility is the bond between the C and the O atom of Fe_3O_4/ZnO. The absorption bands at 524.64 cm^{-1} and 796.60 cm^{-1} are assigned to octahedral Fe-O and tetrahedral Fe-O bonds, respectively. Zn-O bond vibrations occurred at 416.62 cm^{-1} and 445.56 cm^{-1}. The presence of C-O, C-H and O-H bonds indicated the presence of a carbon layer derived from glucose. This proves that the Fe_3O_4@ZnO-C nanocomposite has been successfully performed.

3.3. The Analysis of Magnetic Properties

The VSM results were a hysteresis curve used to analyze the magnetic properties of Fe_3O_4@ZnO-C nanocomposite. The hysteresis curve of Fe_3O_4@ZnO-C nanocomposite with variations in carbon mass can be seen in Figure 3 (a). Based on Figure 3 (a), the values of saturation magnetization (Ms), coercive field (Hc), remanent magnetization (Mr), and the ratio of remanent magnetization to saturation magnetization (Mr/Ms) can be seen in Table 2.

Table 2. VSM characterization results

Sample	Ms (emu/g)	Hc (Oe)	Mr (emu/g)	Ratio (Mr/Ms)	Hmax (kOe)
Fe_3O_4	68.10	40.22	7.22	0.106	10.000
Fe_3O_4@ZnO	66.38	44.92	5.82	0.129	9.997
Fe_3O_4@ZnO-C (0.2 g)	18.23	92.29	2.17	0.119	20.194
Fe_3O_4@ZnO-C (0.1 g)	19.33	92.90	2.35	0.122	20.188
Fe_3O_4@ZnO-C (0.05 g)	22.05	89.60	2.62	0.119	20.201

From Table 2, the Fe_3O_4@ZnO-C nanocomposite has a narrow curve area for each sample with carbon composition variations of 0.2 g, 0.1 g and 0.05 g of 1.3 kOe.emu/g, 1.4 kOe.emu/g and 1.5 kOe.emu/g, while the coercive fields of Hc are 92.29 Oe, 92.90 Oe and 89.60 Oe, respectively. The saturation magnetization value of Fe_3O_4@ZnO-C nanocomposite decreased with the increasing mass of carbon by 22.05 emu/g, 19.33 emu/g and 18.23 emu/g due to the carbon diamagnetism.

Compared to the VSM measurement results of Fe_3O_4@ZnO nanocomposite (without carbon) in Figure 3 (b), the Ms value and the Hc coercive field are 66.38 emu/gr and 44.92 Oe, a significant decrease in magnetic saturation occurred at this point. However, in biomedical applications, it is reported that low magnetic saturation values are better than high saturation values because tissue damage due to high magnetic fields can be minimized. Salem *et al.* [20] also reported that 23 emu/g of Ms was acquired. In comparison, Sabouri *et al.* [21] reached 5 emu/g to 7.88 emu/g of Ms, and many other studies resulted in low Ms values. Superparamagnetic materials with low Ms values have the potential to be developed as photothermal therapy and drug delivery system.

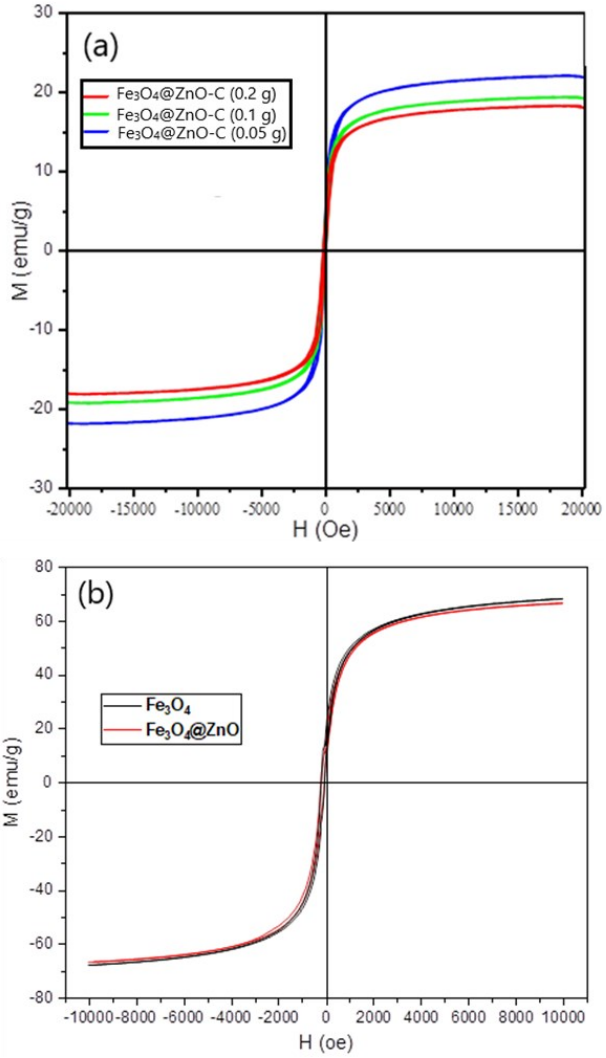

Figure 3. Hysteresis curves of (a) Fe_3O_4@ZnO-C, (b) Fe_3O_4@ZnO and Fe_3O_4 nanocomposites

4. Conclusion

According to the study results on the synthesis and magnetic characterization of Fe_3O_4@ZnO-C nanocomposites using the coprecipitation method, it can be concluded that the synthesis of Fe_3O_4@ZnO-C nanocomposite with variations in carbon mass was successfully conducted, proved by XRD and FTIR results. Fe_3O_4@ZnO-C nanocomposite has superparamagnetic properties, and the magnetic saturation value decreases

with increased carbon mass. Based on its magnetic saturation values, Fe_3O_4@ZnO-C nanocomposite can be developed in biomedicine, such as diagnostics and therapies, especially photothermal therapy for cancer cells.

Acknowledgment

This study was funded by PNBP of the Faculty of Mathematics and Natural Sciences of Andalas University with a research contract No: 21/UN.16.03.D/PP/FMIPA/2021.

References

[1] Mingqian Wang, Ying Liang, Zhicheng Zhang, Guohong Ren, Yajun Liu, Shishan Wu, Jian Shen, Ag@Fe_3O_4@C nanoparticles for multi-modal imaging-guided chemo-photothermal synergistic targeting for cancer therapy, *Analytica Chimica Acta*, 1086, (2019), 122-132 https://doi.org/10.1016/j.aca.2019.08.035

[2] Ming Wu, Da Zhang, Yongyi Zeng, Lingjie Wu, Xiaolong Liu, Jingfeng Liu, Nanocluster of superparamagnetic iron oxide nanoparticles coated with poly (dopamine) for magnetic field-targeting, highly sensitive MRI and photothermal cancer therapy, *Nanotechnology*, 26, 11, (2015), 115102 https://doi.org/10.1088/0957-4484/26/11/115102

[3] Ganeshlenin Kandasamy, Dipak Maity, Recent advances in superparamagnetic iron oxide nanoparticles (SPIONs) for *in vitro* and *in vivo* cancer nanotheranostics, *International Journal of Pharmaceutics*, 496, 2, (2015), 191-218 https://doi.org/10.1016/j.ijpharm.2015.10.058

[4] Juan Pellico, Connor M. Ellis, Jason J. Davis, Nanoparticle-based paramagnetic contrast agents for magnetic resonance imaging, *Contrast Media & Molecular Imaging*, 2019, 1845637, (2019), https://doi.org/10.1155/2019/1845637

[5] Bipin Kumar Gupta, Satbir Singh, Pawan Kumar, Yean Lee, Garima Kedawat, Tharangattu N. Narayanan, Sajna Antony Vithayathil, Liehui Ge, Xiaobo Zhan, Sarika Gupta, Bifunctional luminomagnetic rare-earth nanorods for high-contrast bioimaging nanoprobes, *Scientific Reports*, 6, 1, (2016), 1-12 https://doi.org/10.1038/srep32401

[6] Xinyu Zhao, Qi Yu, Jun Yuan, Nitish V. Thakor, Mei Chee Tan, Biodegradable rare earth fluorochloride nanocrystals for phototheranostics, *RSC Advances*, 10, 26, (2020), 15387-15393 https://doi.org/10.1039/D0RA00760A

[7] V. Madhubala, T. Kalaivani, Phyto and hydrothermal synthesis of Fe_3O_4@ZnO core-shell nanoparticles using *Azadirachta indica* and its cytotoxicity studies, *Applied Surface Science*, 449, (2018), 584-590 https://doi.org/10.1016/j.apsusc.2017.12.105

[8] Jagriti Gupta, P. A. Hassan, K. C. Barick, Core-shell Fe_3O_4@ ZnO nanoparticles for magnetic hyperthermia and bio-imaging applications, *AIP Advances*, 11, 2, (2021), 025207 https://doi.org/10.1063/9.0000135

[9] Xiaoli Liu, Hui Jiang, Jing Ye, Chunqiu Zhao, Shengping Gao, Changyu Wu, Changhui Li, Jincheng Li, Xuemei Wang, Nitrogen - doped carbon quantum dot stabilized magnetic iron oxide nanoprobe for fluorescence, magnetic resonance, and computed tomography triple - modal in vivo bioimaging, *Advanced Functional Materials*, 26, 47, (2016), 8694-8706 https://doi.org/10.1002/adfm.201603084

[10] Roberto Gonzalez-Rodriguez, Elizabeth Campbell, Anton Naumov, Multifunctional graphene oxide/iron oxide nanoparticles for magnetic targeted drug delivery dual magnetic resonance/fluorescence imaging and cancer sensing, *PLoS ONE*, 14, 6, (2019), e0217072 https://doi.org/10.1371/journal.pone.0217072

[11] Ilana Perelshtein, Nina Perkas, Shai Rahimipour, Aharon Gedanken, Bifunctional Carbon Dots—Magnetic and Fluorescent Hybrid Nanoparticles for Diagnostic Applications, *Nanomaterials*, 10, 7, (2020), 1384 https://doi.org/10.3390/nano10071384

[12] Hoang Nguyen, Eric Tinet, Thierry Chauveau, Frédéric Geinguenaud, Yoann Lalatonne, Aude Michel, Rachida Aid-Launais, Clément Journé, Caroline Lefèbvre, Teresa Simon-Yarza, Bimodal fucoidan-coated zinc oxide/iron oxide-based nanoparticles for the imaging of atherothrombosis, *Molecules*, 24, 5, (2019), 962 https://doi.org/10.3390/molecules24050962

[13] Vlasta Zavisova, Martina Koneracka, Jozef Kovac, Martina Kubovcikova, Iryna Antal, Peter Kopcansky, Monika Bednarikova, Marta Muckova, The cytotoxicity of iron oxide nanoparticles with different modifications evaluated in vitro, *Journal of Magnetism and Magnetic Materials*, 380, (2015), 85-89 https://doi.org/10.1016/j.jmmm.2014.10.041

[14] Yong Hu, Ruizhi Wang, Shige Wang, Ling Ding, Jingchao Li, Yu Luo, Xiaolin Wang, Mingwu Shen, Xiangyang Shi, Multifunctional Fe_3O_4@ Au core/shell nanostars: a unique platform for multimode imaging and photothermal therapy of tumors, *Scientific Reports*, 6, 1, (2016), 1-12 https://doi.org/10.1038/srep28325

[15] Vu Minh Thanh, Nguyen Thi Huong, Dao The Nam, Nguyen Dinh Tien Dung, Minh-Tri Nguyen-Le, Synthesis of Ternary Fe_3O_4/ZnO/Chitosan Magnetic Nanoparticles via an Ultrasound-Assisted Coprecipitation Process for Antibacterial Applications, *Journal of Nanomaterials*, 2020, 8875471, (2020), https://doi.org/10.1155/2020/8875471

[16] Alexey Maximenko, Joanna Depciuch, Natalia Łopuszyńska, Malgorzata Stec, Żaneta Świątkowska-Warkocka, Vadim Bayev, Piotr M. Zieliński, Jaroslaw Baran, Julia Fedotova, Władysław P. Węglarz, Fe_3O_4@SiO_2@Au nanoparticles for MRI-guided chemo/NIR photothermal therapy of cancer cells, *RSC Advances*, 10, 44, (2020), 26508-26520 https://doi.org/10.1039/D0RA03699D

[17] M. Reaz, Ariful Haque, D. M. Cornelison, A. Wanekaya, R. Delong, K. Ghosh, Magneto-luminescent zinc/iron oxide core-shell nanoparticles with tunable magnetic properties, *Physica E: Low-dimensional Systems and Nanostructures*, 123, (2020), 114090 https://doi.org/10.1016/j.physe.2020.114090

[18] Sadang Husain, Suryajaya Suryajaya, Ninis Hadi Haryanti, Tetti Novalina Manik, Rodiansono Rodiansono, Sepfina Monica Hutasoit, Agus

Riyanto, Sudarningsih Sudarningsih, Potensi Nanokomposit Fe_3O_4@C dari Bijih Besi Sebagai Pendeteksi Kadar Glukosa, *Positron*, 9, 2, (2019), 44-52

[19] Syamsul Bahtiar, Ahmad Taufiq, Sunaryono Sunaryono, Preparasi dan Karakteristik Struktur Nanokomposit Fe_3O_4/ZnO dengan Menggunakan Metode Kopresipitasi, *Seminar Nasional Fisika dan Pembelajarannya*, 2017

[20] Mohamed L. Salem, Ali Gemeay, Soha Gomaa, Maha A. Aldubayan, Lobna Assy, Superparamagnetic graphene oxide/magnetite nanocomposite delivery system for doxorubicin-induced distinguished tumor cell cycle arrest and apoptosis, *Journal of Nanoparticle Research*, 22, 8, (2020), 1-12 https://doi.org/10.1007/s11051-020-04932-5

[21] Z. Sabouri, S. Labbaf, F. Karimzadeh, A. Baharlou-Houreh, T. V. McFarlane, M. H. Nasr Esfahani, Fe_3O_4/bioactive glass nanostructure: a promising therapeutic platform for osteosarcoma treatment, *Biomedical Materials*, 16, 3, (2021), 035016 https://doi.org/10.1088/1748-605X/aba7d5